Investigation of Trap-Assisted Tunneling Currents in Capacitive Micromachined Ultrasonic Transducers (CMUT) with Silicon Nitride Membranes

Chukwuebuka Okoro, Sazzadur Chowdhury
Department of Electrical and Computer Engineering
University of Windsor
Windsor, Ontario, Canada
E-mail: okoro3@uwindsor.ca, Sazzadur@uwindsor.ca

Abstract—**The results of a theoretical investigation of Poole-Frenkel and 3D Hartke models to predict tunneling currents due to electron emissions from trap centers in silicon nitride membranes in Capacitive Micromachined Ultrasonic Transducers (CMUTs) are presented. A CMUT, with a 0.5 micrometer thick silicon nitride membrane suspended over a 600 nanometer thick vacuum gap was used in the study. The study revealed that the Poole-Frenkel model overestimated electron current densities caused by emissions from silicon nitride trap centers by more than 99% in comparison to the Hartke model prediction. This was observed for a DC bias voltage range of 11-77 volts. This significant variation in predicted current densities is primarily due to the inclusion of multi-directional emission paths in the Hartke model. In contrast, the Poole-Frenkel model considers emissions only in one direction. The study provides valuable insights into the dielectric charging mechanisms in CMUTs, which can aid in the development of solutions to enhance their reliability by minimizing dielectric charging.**

Keywords- Trap-assisted Tunneling; Current Density; Hartke; Poole-Frenkel; CMUT; Silicon nitride; Dielectric Charging.

I. INTRODUCTION

Capacitive Micromachined Ultrasonic Transducers (CMUTs) rely on electrostatically or acoustically forced vibration of a microfabricated membrane suspended over a sealed vacuum cavity to transmit or receive ultrasound [1]. The CMUTs offer attractive functional characteristics, such as higher fractional bandwidth, lower mechanical impedance, lower internal loss, better thermal dissipation, low cost batch fabrication capability, and easier integration with microelectronic integrated circuits to achieve better signal-to-noise ratio that are superior to the conventional piezoelectric transducers [2]–[7].

The CMUTs are particularly envisioned to overcome the limitation of piezoelectric transducers for high-resolution 2D and 3D non-ionizing multi-modal biomedical and Non-Destructive Evaluation (NDE) applications [8]–[14]. Leveraging cost-effective advanced lithography along with precise micro and nanoscale deposition and etching techniques, it is now feasible to fabricate high-frequency linear, planar, non-planar, and flexible CMUT arrays [1].

As the CMUTs and microelectronic Integrated Circuits (ICs) are fabricated using similar microfabrication processes, the CMUTs can easily be integrated with microelectronic ICs to realize 3D-integrated ultrasound microsystems [13]. Such microsystems, by incorporating both the transducers and processing electronics as chiplets in a multifunctional System-In-Package (SIP), can provide high-quality data with a better Signal-to-Noise Ratio (SNR) due to shorter vertical interconnection paths and smaller in-plane routing distance. Examples of such advanced capabilities include dual-mode operation [14], e.g., the same array performing imaging and High-Intensity Focused Ultrasound (HIFU) for conventional therapy, histotripsy (non-thermal tissue ablation), ultrasound elastography, catheter-based invasive high frequency probing of internal body organs, and transparent arrays for 2D and 3D photoacoustic imaging [8]–[15]. Thus, the CMUTs unfold a new set of advanced functionalities that are not achievable with conventional piezoelectric transducers.

Despite these excellent competitive edges, approximately a quarter of a century after their invention in 1996, the CMUTs are still struggling to become the choice of technology in the industries due to some serious reliability issues, of which the electrostatic instability [1], [16]–[18], specifically the dielectric charging phenomena, is considered to be the most serious.

The dielectric charging phenomenon in CMUTs refers to the gradual accumulation of tunneled or trapped charges within the dielectric structural layer of the CMUT membrane, which limits the long-term reliability of the CMUTs. The studies in [1], [16]–[18] categorically noted that the dielectric charging problem in CMUTs must be resolved for the main stream adoption of CMUTs in the biomedical and NDT fields.

The authors in [18] categorized the dielectric charging mechanism in CMUTs into two primary modes: contact charging and non-contact charging. The contact charging mode is triggered when the CMUT membrane collapses on to the backplate as the electrostatic force originating from the applied voltages exceeds the collapse threshold. This leads to a high electric field near the contact interface; promoting aggressive charge injection and dipole alignment (two equal and opposite charges orient themselves due to the applied electric field). This accelerates performance degradation.

The non-contact charging occurs when the CMUT membrane remains suspended without collapsing into the dielectric layer. In this case, charges arise due to internal defects, migration of free charges, and dipole reorientation within the dielectric materials.

In [18], the authors investigated the dominant electrical transport mechanism in typical dielectric materials, silicon nitride and silicon dioxide, used to fabricate CMUT membrane and support posts. The investigation utilized established charge transport models and employed parametric analysis in addition to a dual mode classification of charging mechanism in CMUT materials and geometries. The analysis revealed that membrane thickness, cavity height, thickness of the bottom insulating layer, and the operating temperature, significantly contribute to the dielectric charging phenomenon in CMUTs, providing a better understanding of CMUT charging behavior, aiding in improved design strategies.

Recent studies suggest that the quantum tunneling effect and internal Schottky effect are significant contributors to this charge injection and trapping under high electric fields [19][20]. The Poole-Frenkel (PF) [21]–[23] and Hartke [24][25] models, are two widely used theoretical frameworks to predict trap-assisted charging current density in CMUTs with silicon nitride membranes. On the other hand, the Fowler-Nordheim model [26] is commonly used to predict the charging current density due to the quantum tunneling [19] of charges from the metal electrode to the silicon nitride structural layer in a CMUT membrane.

Silicon nitride is a common dielectric structural material used to fabricate CMUT membranes due to its highly attractive mechanical properties and ease of fabrication. However, the silicon nitride membranes inherently contain structural defects, known as *K*-center defects [21]–[23]. These defects arise during thinfilm deposition processes or from high electric field-induced stress, and they act as charge-trapping sites capable of capturing both electrons and holes [21]–[23]. Under a strong electric field, these trapped charges can be thermally or field-activated to escape into the conduction band, a process known as field-enhanced thermal emission or the Poole-Frenkel (PF) effect [21]–[23].

In the PF model, the applied electric field reduces the Coulombic potential barrier of the trap, thereby enhancing the likelihood of charge emission along the field direction [20]. However, the PF model considers the field-induced potential barrier lowering only in one dimension and does not account for multi-directional emission paths.

On the other hand, the Hartke model extends this concept into three dimensions by averaging the field-lowered barrier over all possible emission angles, thereby offering a more accurate depiction of emission behavior in real materials. This is particularly significant at submicron dielectric thicknesses, which are typical in CMUTs, where charge injection and release occur over a distributed field profile [27].

Various design strategies involving variations in materials, geometries, and fabrication methods have been reported to minimize the dielectric charging phenomena in CMUTs. The authors in [28] presented post CMUT device as another solution to the dielectric charging. Post CMUT is composed of isolation posts of dielectric materials instead of a whole layer. In the design, the post isolation was implemented to reduce the surface area of the insulation layer, which significantly reduces the dielectric charging and its adverse effects. Unlike the conventional CMUTs, which showed shifts and shape changes in the current-voltage characteristics curve due to charge movement and trapping under high electric field, the post CMUTs exhibited stable CV characteristics with no noticeable charging or hysteresis even after high voltage cycling/sweep and spiking tests. This stability is attributed to the limited contact area provided by the posts, effectively isolating the dielectric layer and preventing charge accumulation.

In another technique as reported in [29][30], an enhanced insulation design for CMUTs has been presented that employs a deep trench oxidation method to form a centrally located, thermally grown silicon dioxide layer extending approximately 30 μm into the substrate. This effectively minimized the parasitic charging and device capacitance while also improving the breakdown voltage characteristics.

The charging behavior of various dielectric materials was also investigated in [17] with a focus on comparing plasma-enhanced silicon dioxide and plasma-enhanced silicon nitride using CV measurements. The results showed that charging began once the applied stress voltage reached the CMUT's pull-in voltage, and the plasma-enhanced silicon nitride exhibited a higher susceptibility to charge accumulation than the plasma-enhanced silicon dioxide. Further, the presence of both DC and AC voltage during operation led to more significant charging effects than the use of only DC voltage.

In [31], the authors presented experimental measurement data on dielectric charging in SOI CMUTs. The data showed a clear deviation of experimental values from the analytically estimated values of the capacitance changes as a function of AC and DC excitations. This deviation was attributed to the trapped charges in the silicon-on-insulator layer induced by the strong electric field. The measured capacitance values, which were 4–10 times higher than the estimated value, showed clear evidence of the charging in the dielectric layer. Additionally, the charging effect intensified with an increasing bias voltage. This approach presents a sound interpretation of dielectric charging mechanisms and advances CMUT design by introducing structural pathways for improving the device reliability.

Another highly reliable hexagonal shape CMUT cell structure with a diameter of 60 μm and cavity height of 100 nm was studied in [17], to address the issue of dielectric charging during high voltage operation. The study employed a 200 nm thick PECVD silicon nitride structural layer to form the CMUT membrane. Mechanical spacers or bumps were strategically positioned below the vibrating membrane, along with partial openings in the top membrane directly above these spacers. The primary function of the spacers is to physically limit the membrane's downward displacement, thereby preventing full contact with the bottom cavity surface even when the applied driving voltage exceeds the device collapse voltage. By constraining the membrane to substrate contact area, the structure effectively minimizes current leakage through the dielectric during transient contact events, enhancing dielectric integrity. Furthermore, the introduction of partial electrode openings serves to reduce local electric field intensities at the regions of minimal electrode separation, particularly above each spacer. This redistribution of the field significantly improves the dielectric reliability of the CMUT cells compared to conventional configurations. Long-term experimental measurements as reported in [17] demonstrated that the proposed structure maintained stable receiving sensitivity, with fluctuations remaining below 1dB after more than 6×10^{11} membrane vibration cycles at voltages beyond collapse. Additionally, the design enabled a three times increase in transmitted acoustic pressure under the same driving conditions, indicating substantial performance gains. Collectively, these enhancements make the structure highly suitable for demanding medical imaging applications, where both high output and long-term reliability are critical.

In this context, this paper investigates both Poole-Frenkel and Hartke models predicted current densities in the context of CMUTs with silicon nitride membranes. The investigation results can be used for more accurate design of CMUTs to improve their reliability by decreasing the trap-assisted dielectric charging effects.

The remainder of this paper is structured as follows: Section II provides the operational and material aspects of a CMUT, Section III outlines the theoretical models governing field-induced barrier lowering and electron emission in CMUTs with silicon nitride membranes, Section IV presents the results of MATLAB-based analytical modeling, Section V provides a brief analysis of charging current density variation based on nitrogen composition, and finally Section VI provides the concluding remarks.

II. CMUT Operation and Material Considerations

The CMUT is a reciprocal electrostatic transducer. The cross-section of a typical CMUT geometry is shown in Figure 1. As Figure 1 shows, a CMUT geometry is constructed to have a flexible membrane at the top, which is anchored around its edges by dielectric support posts and suspended over a vacuum cavity formed between the top membrane and a fixed bottom plate [1]. The geometry essentially constituents a variable capacitor where the top membrane acts as a deformable upper electrode and the fixed plate at the bottom acts as the fixed bottom electrode. In some implementations, a thin insulating layer is added on the top of the bottom electrode to prevent device damage during a collapse mode operation. The top membrane is constructed with a highly doped single crystal silicon layer, or a functionalized dielectric structural layer such as silicon nitride or a suitable polymer.

A. 2.1 CMUT Operation

Approximating the CMUT geometry as a parallel plate variable capacitor as shown in Figure 2, if the upper plate is displaced by a distance x, the resulting capacitance of the structure can be expressed as

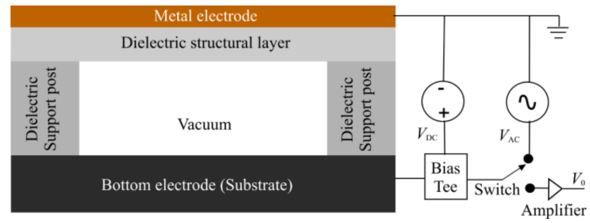

Figure 1. A cross-section of a CMUT and its typical operational setup.

$$C = \varepsilon_0 \varepsilon_r \frac{A}{(g_{eff} - x)} \quad (1)$$

and the effective plate gap height g_{eff} can be expressed as

$$g_{eff} = \frac{t_i}{\varepsilon_r} + \frac{t_m}{\varepsilon_m} + g_0 \quad (2)$$

In (1) and (2), A is coupling area of the capacitor plates, ε_0, ε_r ,and ε_m are the permittivities of free space, the bottom insulating layer, and the membrane structural material, respectively, g_0 is the initial gap between capacitor plates, x is the membrane deflection, t_m, and t_i are the membrane and insulator thickness, respectively.

The mechanical behavior of this configuration can be described using Newton's equation of motion as [32]

$$m\frac{d^2x}{dt^2} + b\frac{dx}{dt} + kx = F \quad (3)$$

In (3), F is the actuating force (electrostatic or acoustic) m is the mass of the movable plate, k is stiffness of the movable plate, and b represents the damping parameter of the system.

The CMUT operates both as a transmitter to emit ultrasound in the medium and also as a receiver to generate an electric signal in response to an incident ultrasound wave.

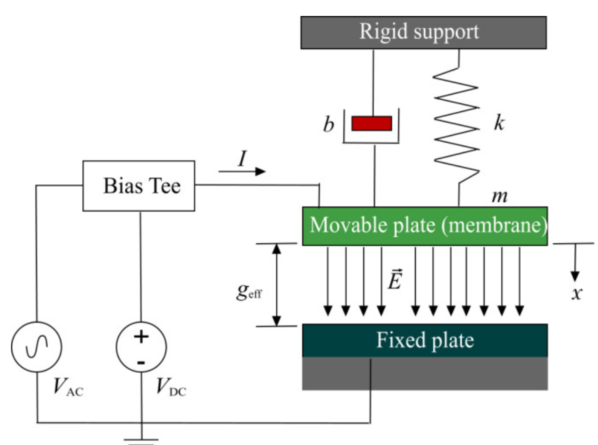

Figure 2. Electromechanical model of a CMUT.

A control signal operates a switch to enable mode switching as shown in Figure 1.

In the transmit mode, an AC voltage of desired frequency and amplitude, superposed with a suitable DC bias voltage, is applied across the CMUT geometry as shown in Figure 1. The resulting time-varying electrostatic attraction force between the CMUT electrodes (top membrane and the fixed bottom electrode) causes the membrane to vibrate and generate ultrasound waves in the medium.

During the receiving mode, an incident ultrasound wave forces the membrane to vibrate at the incident wave frequency. This vibration of the membrane dynamically alters the gap between the membrane and the bottom electrode, which affects a change in CMUT capacitance. This capacitance change is converted to an output voltage using a suitable microelectronic circuit.

Due to the fundamentally different physical principles of operation, ability to detect nano and picoscale precision variations of operational parameters (e.g., membrane displacement), and high precision microfabrication capabilities, CMUT transmit and receive performances are much superior compared to their piezoelectric counter parts. A comparison of some of the key performance parameters of CMUTs and piezoelectric transducers are provided in Table I.

B. *CMUT Membrane Material*

The mechanical and electrical properties of the CMUT membrane material are crucial to obtain the necessary output pressure (transmit operation) and generated voltage (receive operation). Common materials to fabricate the CMUT membranes are listed below with their relative advantages and disadvantages.

TABLE I. CMUT AND PZT PERFORMANCE COMPARISON [33].

S/N	Parameter	CMUT	PZT
1	Fabrication Method	Wafer bonding, surface micromachining, bulk micromachining	DF (Dice and Fill), Laminating
2	Array fabrication	Low cost	Expensive
3	Frequency range	1MHz - >100MHz	Comparatively small 50 kHz to 20MHz
4	Bandwidth	Wider fractionnal bandwidth (>100%)	Narrower Bandwidth
5	Output pressure for a similar voltage level	Comparatively low but improving	High
6	IC integration	Can be integrated easily with front-end electronics	Comparatively difficult to integrate with front-end electronics
7	Thermal stability	High thermal stability	Low thermal stability
8	Frequency use	Easier high-frequency fabrication	Difficult high-frequency fabrication
9	Sensitivity (mV/kPa)	22.57	4.28
10	DC bias	Required	N/A
11	SNR (dB)	22–87	18–22

Single crystal silicon: This method uses a thin layer of single-crystal silicon, typically the device layer of an SOI (silicon-on-insulator) wafer or a bulk micromachined silicon wafer, to realize the CMUT membrane. The objective is to achieve a desired level of electrical conductivity by doping and mechanical strengths for the membrane to attain target vibrational characteristics, optimal membrane deflection, and electrostatic actuation forces. However, the SOI wafers are expensive, and the thickness uniformity of the device layer remains a challenging issue.

Polycrystalline silicon (polysilicon): Polysilicon offers similar benefits and issues as the single-crystal silicon. However, as the suspended polysilicon membranes are realized using a Low-Pressure Chemical Vapor Deposition (LPCVD) method in a surface micromachining process, the realization of a suspended membrane using a sacrificial layer creates fabrication complexity, non-perfect geometry, and involves additional manufacturing cost.

Polymers and Metals: Various types of polymers such as Benzocyclobutene (BCB), SU-8, or Parylene-C are becoming popular to realize CMUT membranes using a wafer-bonded process. The polymer layers are functionalized with a thin metal layer, typically gold, deposited at the top or at the bottom of the membrane. Polymers contribute flexibility and structural resilience, while the metal layer as a high-conductivity electrode. Due to the high flexibility of the polymer membranes, it is possible to obtain high deflection during acoustical or electrical actuation. The polymer membranes can be realized using a simple spin deposition technique at a low cost.

Ceramics and metals: Ceramics (e.g., Silicon nitride, 3H-SiC) offer high mechanical strength and durability, facilitating reliable membrane vibration over a longer period [31]. Microfabricated (both surface micromachined and wafer bonded) silicon nitride thinfilms, specifically stoichiometric silicon nitride (Si_3N_4) functionalized with gold thinfilms, are widely used to fabricate CMUT membranes due to their high mechanical strength and low residual stress.

A comparative review in [34] revealed that ceramic materials exhibit superior performance when optimizing both diaphragm deflection and resonant frequency simultaneously, significantly outperforming metallic and polymer alternatives. The analysis in [34] that used a wide set of materials indicated that among all materials evaluated, only 3H-SiC, silicon nitride, and silicon with (110) crystal orientation surpass the performance characteristics of conventional silicon membranes. While silicon nitride membranes demonstrate the highest load-deflection characteristics, the dielectric charging phenomena in silicon nitride membranes is a critical issue that seriously compromises the operational reliability of CMUTs. Most importantly, the dielectric charging phenomena in silicon nitride membranes causes a drift of their resonant frequency from the designed value and vibrational characteristics due to a spring softening effect [32]. While the issue of dielectric charging in silicon nitride MEMS switches is being investigated by various researchers [21], the dielectric charging issues in CMUTs with silicon nitride membranes is a much less explored area.

C. Silicon Nitride as CMUT Membrane Material

Silicon nitride is a hard material from the family of ceramics consisting of silicon and nitrogen [35]. Bulk silicon nitride is produced from materials compositions such as silicon powder (starting raw material), beta silicon nitride powder (diluting agent), high purity nitrogen, sodium chloride (molten salt) as listed in [35]. It has been observed in [35] that the nitridation of silicon with sodium chloride (NaCl) additives yielded two distinct product layers, which include the upper fibrous layer (impurities) and lower blocky layer (pure Si_3N_4). Also at 1250°C-1350°C a mixture composition of α-Si_3N_4, β-Si_3N_4 and silicon was seen but the silicon vanished at 1350°C making α-Si_3N_4 the dominant constituent.

Microfabricated silicon nitride thinfilms are typically deposited using two primary methods: Low Pressure Chemical Vapor Deposition (LPCVD) and Plasma-Enhanced Chemical Vapor Deposition (PECVD) [36][37]. While both techniques are extensively utilized across various applications, they differ in deposition rates and film quality. LPCVD operates at a slower pace, whereas PECVD enables faster film formation [37]. Further, as the LPCVD method realized silicon nitride films are stoichiometric (Si_3N_4) in nature with significantly low residual stress compared to PECVD method realized nitrides (SiN), the stoichiometric silicon nitride (Si_3N_4) is preferred to realize CMUT membranes. A comparison of physical properties of both types of thinfilm silicon nitrides are provided in Table II [37].

TABLE II. COMPARISON OF SELECTED PHYSICAL PROPERTIES OF LPCVD AND PECVD SILICON NITRIDE THINFILMS [37].

Property	LPCVD	PECVD	Unit
Deposition temperature	973–1073	473–673	K
Particles	Few	Many	
Step coverage	Conformable	Poor	
Dielectric constant	6–7	6–9	
Residual stress	1T	2C-5T	10^8 N/m
Young's modulus	270	300	GPa
Film quality	Excellent	Poor	
Dielectric strength	10	5	10^8 V/m
Resistivity	10^{14}	$10\text{-}10^{13}$	Ω-m

Note: C = compressive; T = tensile.

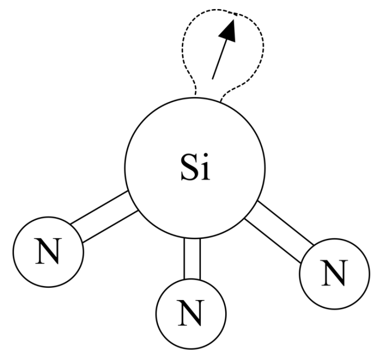

Figure 3. Formation of silicon nitride dangling bond as a silicon atom bonds with 3 nitrogen atom with one dangling bond ($Si \equiv N$) [22].

III. PHYSICS OF DIELECTRIC CHARGING IN SILICON NITRIDE THINFILMS

The fundamental physical laws of dielectric charging in silicon nitride thinfilms have been investigated by many researchers [3][21][22][29][30].

A. K-center Defects in Silicon Nitride Thinfilms

The dielectric charging phenomenon in both N-rich PECVD and stoichiometric silicon nitride (Si_3N_4) thinfilms mainly is attributed to the $Si \equiv N$ dangling bonds (defined as an unpaired electron of a silicon atom that is bonded to three nitrogen atoms [21][22][38]). These $Si \equiv N$ dangling bonds form energy states that can trap either holes or electrons as shown conceptually in Figure 3 [21]. Known as *K*-center defects, these traps are characterized as amphoteric trap centers (can capture both electrons and holes) with a trap energy state of approximately 4.2eV for a silicon dangling bond just under the conduction band minimum and -2eV for nitrogen dangling bond near the valence band minimum in silicon nitride [23]. This suggests that the nitrogen dangling bond makes no significant contribution to charge trapping, as it forms a state outside the band gap.

Following [22], due to strong negative electron-electron correlation energy, *K*-center with two spins (↑↓) is energetically more stable than the neutral *K*-centers (K^0) with single spin of electron (↑), making the neutral *K*-centers (K^0) more stable. As electrons are injected into either N-rich PECVD or stoichiometric silicon nitride thinfilms, they can be captured by neutral *K*-center (K^0) and become trapped there to make the *K*-center negatively charged ($K^0 + e^- = K^-$).

Similarly, when holes are injected into N-rich PECVD or stoichiometric silicon nitride thinfilms, the neutral *K*-centers (K^0) become positively charged ($K^0 + h^+ = K^+$). The phenomenon is illustrated conceptually in Figure 4. It is to be noted here that while the neutral *K*-centers (K^0) exhibit paramagnetic behavior with an unpaired electron in silicon atom, both positive and negatively charged *K*-center exhibit diamagnetic behavior without any unpaired electron (for hole capture, the unpaired electron is annihilated and for electron capture, two electrons of opposite spin occupies the energy level).

In [38][39], the *K*-center defect densities were measured and quantified using Electron Spin Resonance (ESR) along with Capacitive-Voltage (C-V) measurement technique, and it was discovered that SiN_x films illuminated with high

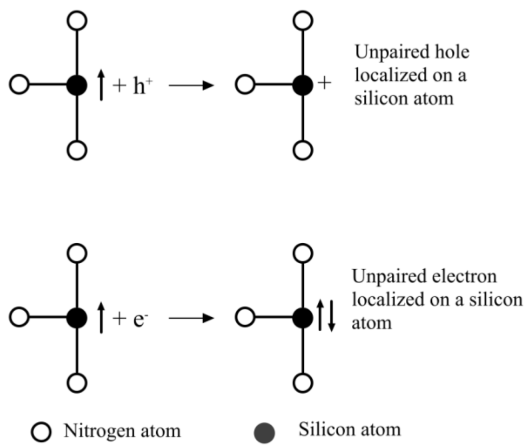

Figure 4. Schematic diagram of the *K*-center showing an unpaired electron localized on a silicon atom and bonded to three nitrogen.

energy UV(~4.9 eV) radiation increased the paramagnetic signal. Based on the measurement, it was concluded that the UV light was able to annihilate all the charges present in the film (K^+ or K^-) and convert them to neutral paramagnetic K^0 states. Further, the authors in [38][40] used an Electron Nuclear Double Resonance (ENDOR) technique to determine the structure of the defects in silicon nitride thinfilms. The investigation discovered that the silicon dangling bond with three nitrogen atoms is the primary defect responsible for charge trapping in the silicon nitride thinfilms. The detailed studies of the charge trapping due to silicon or nitrogen dangling bond is found in [20]–[22],[38].

These trap sites, due to different silicon and nitride composition, exhibit varying defect densities and thereby influencing the charge trapping behaviors, and ultimately the operational reliability of the CMUTs. Therefore, understanding the dielectric properties of silicon nitride and its compositions is essential in evaluating the extent of charge injection and retention during CMUT operation.

The movement of trapped charge carriers that are thermally emitted from the *K*-centers (basically coulombic trap states) into the conduction or valence band of the dielectric material gives rise to a current density. At the same time, charges are injected from the metal electrode to the silicon nitride layer through a tunneling process, contributing to a tunneling current density. Both current densities contribute to dynamically changing charge densities in the CMUT membrane, which forces a dynamic shift in the operating point and resonant frequency of CMUT membrane vibration, which affects the output pressure, vibrational characteristics, and receiving sensitivity [20]. Due to limited scope, this research work is focused on the trapped charge contributed current density in CMUTs with silicon nitride membranes.

B. Field-Induced Barrier Lowering In a CMUT

The potential energy distribution in a typical field emission system comprised of a metal electrode and a dielectric material after applying an electric field is shown in Figure 5 [20].

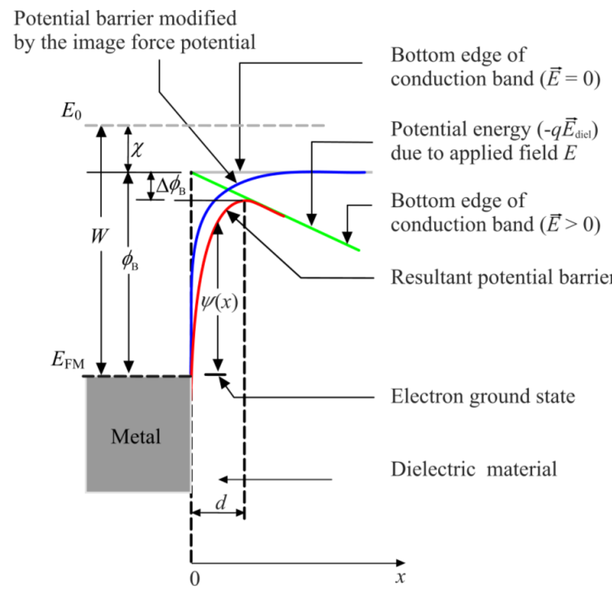

Figure 5. Potential energy barrier lowering in a typical metal-dielectric emission system due to an applied electric field [42].

In Figure 5, E_{FM} is the metal Fermi level, W is metal work function, χ is insulator electron affinity, $\vec{E}$ is applied electric field, d is dielectric thickness, ϕ_B is the potential barrier height, $\Delta\phi_B$ is decrease in potential barrier height, and $\psi(x)$ is the resultant potential barrier.

The potential energy barrier from metal to the dielectric material can be expressed as (4) below [19][21].

$$\psi(x)=\begin{cases}0 & x<0\\ V_0-\chi-q\vec{E}_{\text{diel}}x & 0\le x<d\\ V_0+q(\vec{E}-\vec{E}_{\text{diel}})d-q\vec{E}x & x\ge d\end{cases} \quad (4)$$

This potential energy barrier lowering due to an applied electric field is known as the Schottky effect.

In a dielectric material, such as silicon nitride with trap centers, the electric field due to an applied bias voltage also decreases the height of the potential energy barrier of the trap center (trap depth) in a similar fashion and is known as the internal Schottky effect [20]–[22]. If the potential energy barrier lowering due to the internal Schottky effect is sufficient, a trapped electron can overcome the barrier and be transported to the conduction band with little thermal agitation. As the trapped charges are transported to the conduction band, they contribute to dielectric charging and in turn, a leakage current.

This theoretical framework forms the basis of investigating the dielectric charging of silicon nitride membranes in CMUT due to the *K*-center defects. When a bias voltage is applied across the CMUT electrodes during operation, the internal Schottky effect associated with the electric field lowers the potential barrier of the *K*-center defects in silico nitride membranes, enabling the electrons to overcome the potential barrier related to the traps, and move to the conduction band. A conceptual depiction of this internal Schottky effect-induced barrier lowering in the context of a CMUT is shown in Figure 6, assuming the barrier to have a triangular profile. In Figure 6, the field emission occurs from the top metal electrode surface. The interface between the metal and the stoichiometric Si_3N_4 structural layer of the membrane is positioned at $x = 0$ where d is the thickness of the Si_3N_4 layer.

The metal is characterized by a Fermi level E_{FM}, work function W, and electron affinity χ and ε_r is the relative permittivity of the Si_3N_4 layer.

The initial energy E of an electron at a specific location x along the x-axis is determined by its position x. The electric field $\vec{E}$ due to the bias voltage works across the vacuum gap and the $\vec{E}_{diel}$ represents the electric field in the silicon nitride layer.

For the CMUT geometry in Figure 6, the Poole-Frenkel emission model predicted current density J_{PF} can be calculated using (5) below [21].

$$\left.\begin{aligned} J_{PF} &= C\vec{E}\exp\left(\frac{-\left(\phi-\beta_{PF}\sqrt{\vec{E}}\right)}{k_B T}\right) \\ \beta_{PF} &= \sqrt{\frac{q^3}{\pi\varepsilon_0\varepsilon_r}} \end{aligned}\right\} \qquad (5)$$

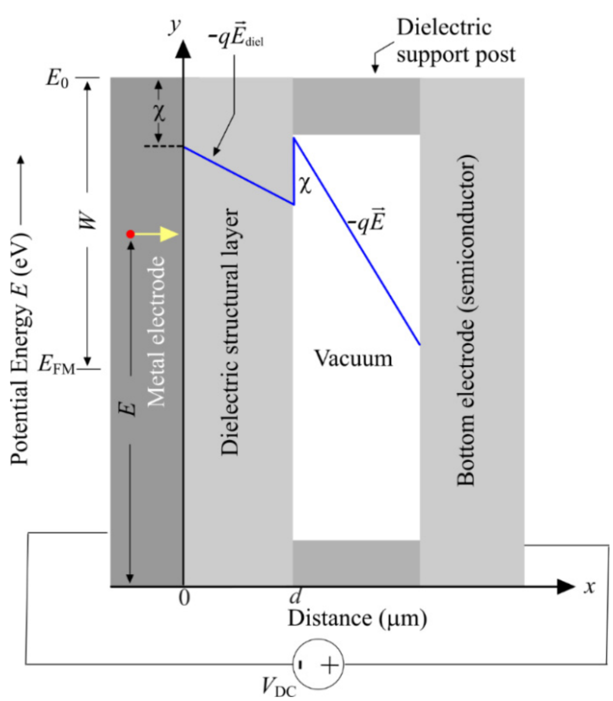

Figure 6. CMUT model showing the triangular barrier lowering due to applied potential energy.

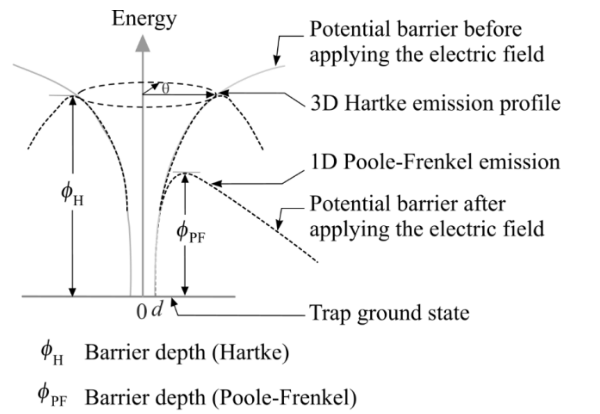

Figure 7. Conceptual diagram showing unidirectional Poole-Frenkel and 3D Hatke models of electron emission due to potential barrier lowering.

In (5), the parameter ϕ is the energy level of the charge trap; C is a pre-exponential factor, β_{PF} is the Poole-Frenkel potential barrier lowering coefficient; ε_0 is the permittivity of free space, ε_r is the relative permittivity of the nitride layer; q is the electronic charge; k_B is the Boltzmann constant and T is the temperature in kelvin. In [42], the value of the pre-exponential factor C has been reported as 0.1 A/V-m for Si_3N_4.

One important feature of the Poole-Frenkel emission model as expressed in (5) is that the model predicted emission current density is unidirectional (e.g., along the *x*-direction as in Figures 5 and 6). However, in reality, charge emissions from the trap centers due to the internal Schottky effect are not unidirectional but occur over a range of directions in a 3D space, as shown conceptually in Figure 7.

The major difference between these two models lies on the fact that unlike the unidirectional Poole-Frenkel emission model, the Hartke emission model accounts for the internal Schottky effect in a 3D space by introducing angular dependencies where the barrier lowering varies with an angle θ between the direction of the applied field and the emission path, described as $\Delta\phi\cos\theta$ [24][25]. By integrating this relationship over all possible emission angles, the effective average barrier can be calculated with a higher accuracy. Accordingly, the emission current density resulting from the electric field due to the CMUT bias voltage following the Hartke model can be expressed as [24][25]

$$\left.\begin{aligned} J_H &= \exp\left(\frac{-\phi}{k_B T}\right)\left(\frac{k_B T}{\Delta\phi\sqrt{\vec{E}}}\right)^2 \\ &\times\left(1+\left(\left(\frac{\Delta\phi\sqrt{\vec{E}}}{k_B T}\right)-1\right)\exp\left(\frac{\Delta\phi\sqrt{\vec{E}}}{k_B T}\right)\right)+\frac{1}{2} \\ \Delta\phi &= \sqrt{\frac{q^3}{\pi\varepsilon_0\varepsilon_r}} \end{aligned}\right\} \qquad (6)$$

where $\Delta\phi$ is the barrier-lowering coefficient and other parameters remains the same as in (5).

The authors in [24][25] reported that the 3D Hartke model predicted barrier-lowering amount is less than the maximum values predicted by the 1D Poole-Frenkel model. Thus, the unidirectional (1D) Poole-Frenkel model calculated emission current in a CMUT with a silicon nitride membrane is expected to deviate from the values calculated using the more realistic 3D Hartke model. This deviation is particularly significant at submicron dielectric thicknesses, which are typical in CMUTs, where charge injection and release occur over a distributed field profile [25].

IV. RESULTS

Matlab-based analytical modeling was conducted to compare the 1D Poole-Frenkel model with the 3D Hartke model. A CMUT geometry with a gold-coated silicon nitride membrane has been used for the comparison. The cross-section of the CMUT geometry is the same as in Figure 1. The CMUT specifications are listed in Table III.

TABLE III. CMUT SPECIFICATIONS.

Parameters	Dimension	Unit
Top electrode thickness (gold)	0.4	µm
Silicon nitride (Si_3N_4) structural layer thickness	0.5	µm
Vacuum gap thickness	0.6	µm
Bottom electrode thickness (silicon)	0.5	µm
Gap between electrodes	1.1	µm
Temperature	300	K

Figure 8 shows the Poole-Frenkel model predicted current density J_{PF} as a function of the electric field $\vec{E}$ due to an applied DC bias voltage. As Figure 8 reveals, the Poole-Frenkel current density J_{PF} increases rapidly as the effective barrier height decreases with an increasing electric field.

Figure 9 shows the Hartke model predicted current density J_H as a function of the electric field $\vec{E}$ due to an applied DC bias voltage.

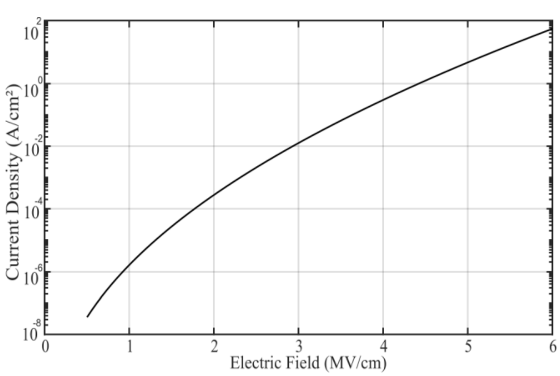

Figure 8. Poole-Frenkel emission model predicted current density due to the trap centers in the CMUT silicon nitride membrane as a function of the electric field associated with the CMUT bias voltage.

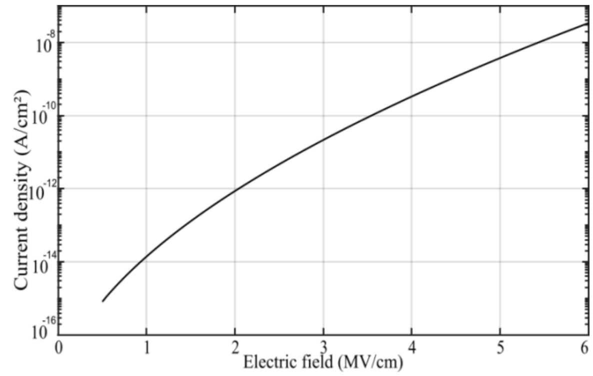

Figure 9. 3D Hartke model predicted current density due to the trap centers in the CMUT silicon nitride membrane as a function of the electric field associated with the CMUT bias voltage.

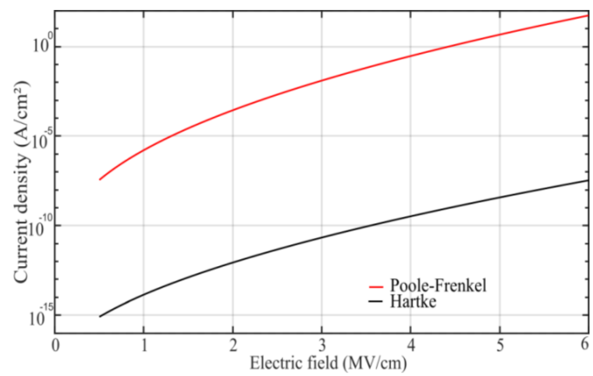

Figure 10. Comparison of Hartke and Poole-Frenkel emission models predicted current densities.

As expected, the Hartke model predicted current density also increases rapidly as the electric field due to the CMUT bias voltage increases due to a lowering of the barrier height. Figure 10 compares the current densities predicted by both the models for the same CMUT geometry subject to the same bias voltage variations. The percent variations in the current densities predicted by both models are tabulated in Table IV.

As Table IV shows, the Poole-Frenkel model predicted current density consistently predicts higher current densities compared to those predicted by the Hartke model by more than 99% for a bias voltage range of 11V-77V.

TABLE IV. CURRENT DENSITY COMPARISON.

Bias Voltage (V)	Hartke model current density, J_H (A/cm^2)	Poole-Frenkel model current density J_{PF} (A/cm^2)	Δ% $\frac{J_{PF}-J_H}{J_{PF}}\times100$
11	2.689×10^{-12}	1.077×10^{-10}	97.5
22	8.154×10^{-12}	8.771×10^{-10}	99.0
33	2.016×10^{-11}	3.864×10^{-9}	99.47
44	4.425×10^{-11}	1.277×10^{-8}	99.65
55	8.950×10^{-11}	3.555×10^{-8}	99.83
66	1.704×10^{-10}	8.796×10^{-8}	99.80
77	3.099×10^{-10}	1.996×10^{-7}	99.84

V. Current Density Variation Based on Nitrogen Composition

As the trap density in a silicon nitride layer depends on the actual composition of silicon and nitrogen in N-rich PECVD or stoichiometric LPCVD silicon nitride thinfilms, it is worth investigating the current densities as a function of silicon and nitrogen composition. To conduct this investigation, three different silicon nitride layers with varying silicon and nitrogen compositions as listed in Table V were used [42]. Corresponding current densities as a function of bias voltage associated electric field are plotted in Figure 11. As it can be seen in Figure 11, the layer with the lowest nitrogen content has lower trap depth and, consequently, higher emission current density for the same electric field.

TABLE V. Different LPCVD Silicon Nitride Compositions With Corresponding Trap Depths [42].

Composition	Trap depth/ionization potential ϕ (eV)
$SiN_{0.75}$	0.56
$SiN_{1.17}$	0.92
$SiN_{1.22}$	1.13

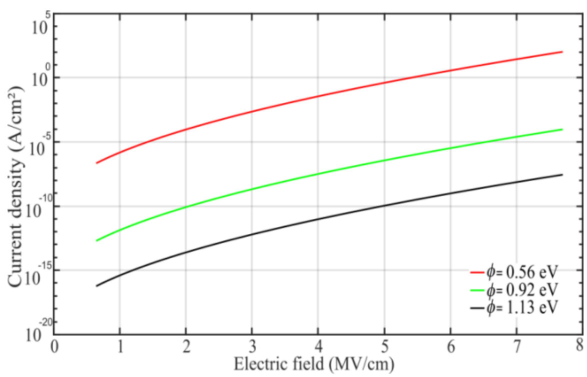

Figure 11. The Hartke model predicted current densities for three different silicon nitride layers with varying composition of silicon and nitrogen and trap depth energy levels as listed in Table V.

VI. Conclusions

The investigation revealed that in a CMUT geometry with silicon nitride membranes, the Poole-Frenkel model consistently predicts emission current densities that are more than 99% higher than those predicted by the Hartke model within a bias voltage range of 11–77 volts. To provide a context, a theoretical study published in [25] concluded that the unidirectional (1D) Poole-Frenkel model consistently predicted a 66% higher emission rate compared to the 3D Hartke model for two plane parallel electrodes separated by a dielectric medium. Obviously, the Poole-Frenkel model overestimates the emission current.

Apparently, this is due to its assumption of a one-dimensional potential barrier lowering. However, the Hartke model, which takes into account the three-dimensional nature of the *K*-center traps, aligns more closely with actual trap behavior. It can be concluded that, in comparison to the Poole-Frenkel model, the Hartke model is a more accurate method for predicting the emission current in 3D microstructures, such as a CMUT that uses a vibrating silicon nitride membrane to transmit or receive ultrasound.

Furthermore, the study found that the trap depths (potential barrier height) in a silicon nitride layer that in turn contributes to the extent of the emission current density in a CMUT, is influenced by the specific composition of silicon and nitrogen within the layer. The parameters of the deposition process, such as plasma-enhanced chemical vapor deposition (PECVD) or low-pressure chemical vapor deposition (LPCVD), greatly influence the composition of the deposited materials in a thinfilm. Investigation revealed that as the nitrogen content increases, the energy trap depth also increases. Accordingly, among the 3 investigated silicon nitride layers, the one with the lowest nitrogen concentration (and therefore the lowest energy trap depth of 0.56 eV) results in the highest emission current density at the same electric field strength.

Furthermore, during vibration, the silicon nitride membrane of a CMUT deforms causing distortion of the energy levels of the charge traps located within the membrane. It is thus necessary to evaluate the Hartke model predicted current densities in dynamically vibrating CMUT membranes against experimentally measured values to better understand the dynamic behavior of the physics of trap-assisted emission currents to mitigate their effects.

Acknowledgment

This research work is supported by Natural Sciences and Engineering Research Council of Canada (NSERC)'s Discovery Grant RGPIN-2025-04794 and IntelliSense Corp, 220 Broadway, Suite 102, Lynnfield, MA 01940, USA.

References

[1] C. Okoro and S. Chowdhury, "Comparison of Poole-Frenkel and Hartke Emission Currents in a Capacitive Micromachined Ultrasonic Transducer (CMUT)," in *Proc. of The Sixteenth International Conference on Sensor Device Technologies and Applications* (*SENSORDEVICES 2025*), Barcelona, Spain, 2025, pp. 10-14.

[2] A. Ergun, G. Yaralioglu, O. Oralkan, and B. T. Khuri-Yakub, "Techniques and Applications of Capacitive Micromachined Ultrasonic Transducers," in *MEMS/NEMS Handbook Techniques and Applications,* Vol. 1, Design Methods, C. Leondes, Ed. _ New York: Springer, 2006, pp. 553-615.

[3] R. Manwar, T. Simpson, A. Bakhtazad, and S. Chowdhury, "Fabrication and characterization of a high frequency and high coupling coefficient CMUT array," *Microsystem Technologies*, vol. 23, pp. 4965–4977, Oct. 2017.

[4] M. Klemm, "Acoustic Simulation and Characterization of Capacitive Micromachined Ultrasonic Transducers," Ph.D. Dissertation, Faculty of Electrical Engineering and Information Technology, Technical University of Dresden, Dresden, Germany, 2017.

[5] S. Berg, "Capacitive Micromachined Ultrasonic Transducers–Acoustic Challenges and Proposed Solutions," Ph.D. Dissertation, Department of Electronics and Telecommunications, Norwegian University of Science and Technology, Trondheim, Norway, 2012.

[6] X. Zhang, "Capacitive Micromachined Ultrasonic Transducers (CMUTs) on Glass Substrates for Next–

Generation Medical Imaging and Beyond," Ph.D. Dissertation, Dept. of Electrical and Computer Engineering, North Carolina State University, Raleigh, North Carolina, 2017.

[7] M. Vallet et al., "Quantitative Comparison of PZT and CMUT Probes for Photoacoustic Imaging: Experimental validation," *Photoacoustics*, vol. 8, pp. 48–58, Dec. 2017.

[8] B. Heiles et al., "Ultrafast 3D Ultrasound Localization Microscopy using a 32×32 Matrix Array," *IEEE Transactions on Medical Imaging*, vol. 38, pp. 2005-2015, Apr. 2019.

[9] Z. Xu, "Histotripsy: the First noninvasive, Non-ionizing, Non-thermal Ablation Technique based on Ultrasound," *Int. J Hyperthermia*, vol. 38, pp. 561–575, Apr. 2021.

[10] Focused Ultrasound Foundation, "Focused Ultrasound for Alzheimer's Disease," Charlottesville, VA, 2022.

[11] J. Jang et al., "Dual-Mode Integrated Circuit for Imaging and HIFU With 2-D CMUT Arrays," in *Proc. of 2015 IEEE International Ultrasonics Symposium* (*IUS*), 2015, pp. 1-14.

[12] C. Arvanitis and F. Degertekin, "Multi-Functional Sparse Phased Arrays for Guiding Focused Ultrasound Therapies," US Patent 12 427 344, Sept. 30, 2025.

[13] T. Matéo et al., "A 1-D CMUT transducer with front-end ASIC in a 9 French catheter for intracardiac echocardiography: Acoustic and Imaging evaluation," in *Proc. of 2020 IEEE International Ultrasonics Symposium* (*IUS*), 2020, pp. 1-8.

[14] M. Engholm, "Capacitive Micromachined Ultrasonic Transducers for 3–D Imaging," Ph.D. Disssertation, Department of Micro- and Nanotechnology, Technical University of Denmark, Kongens Lyngby, Denmark, 2018.

[15] M. Schiffer, "Function-Driven Innovation: How Technology Follows the Needs of Chiplet Systems," in *Proc. of Electronic Packaging Day 2025 Conference*, Fraunhofer IZM, Berlin, Germany, November 6-7, 2025, pp. 1-16.

[16] J. Munir, Q. Ain, and H. Lee, "Reliability issue related to dielectric charging in capacitive micromachined ultrasonic transducers: A review," *Microelectronics Reliability*, vol. 92, pp. 155–167, Jan. 2019.

[17] S. Machida, T. Takezaki, T. Kobayashi, H. Tanaka, and T. Nagata, "Highly reliable CMUT cell structure with reduced dielectric charging effect," in Proc. of *2015 IEEE International Ultrasonics Symposium* (*IUS*), 2015, pp. 1-4.

[18] J. Li, Y. Li, and P. Zhang, "Modelling and Analysis of Dielectric Charge of CMUTs," *IOP Conf. Ser.: Mater. Sci.* Eng., vol. 768, pp. 062106, Mar. 2020.

[19] S. Kasap, *Principles of electronic materials and devices,* Fourth edition. New York, NY: McGraw-Hill, 2018, pp. 221-230.

[20] D. Choi, "Numerical Modeling of Space Charge Dynamics And Electrical Breakdown in Solid Dielectrics," Ph.D. dissertation, Department of Materials Science and Engineering, The Pennsylvania State University, University Park, PA, 2013.

[21] A. Dogan, "The Reliability of the Silicon Nitride Dielectric in Capacitive MEMS Switches," Master's thesis, Department of Materials Science and Engineering, The Pennsylvania State University, University park, PA, 2005.

[22] V. Sharma, "Study of Charges Present in Silicon Nitride Thin Films and Their Effect on Silicon Solar Cell Efficiencies," Ph.D. dissertation, Department of Electrical Engineering, Arizona State University, Tempe, AZ, 2013.

[23] J. Simmons, "Poole-Frenkel Effect and Schottky Effect in Metal-Insulator-Metal Systems," *Phys. Rev*., vol. 155, pp. 657-660, Mar. 1967.

[24] J. Hartke, "The Three-Dimensional Poole-Frenkel Effect," *Journal of Applied Physics*, vol. 39, pp. 4871–4873, Sept. 1968.

[25] P. Murgatroyd, "Theory of space-charge-limited current enhanced by Frenkel effect," *J. Phys. D: Appl. Phys*., vol. 3, pp. 151–156, Feb. 1970.

[26] R. Fowler and L Nordheim, "Electron Emission in Intense Electric Fields," *Proc. of the Royal Society of London*, *Series A*, vol. 119, pp. 173-181, 1928.

[27] M. Zubair, Y. Ang, and L. Ang, "Fractional Fowler-Nordheim Law for Field Emission from Rough Surface with Non-parabolic Energy Dispersion," *IEEE Trans. Electron Devices*, vol. 65, pp. 2089–2095, Jun. 2018.

[28] Y. Huang et al., "A solution to the charging problems in capacitive micromachined ultrasonic transducers," *IEEE Trans. Ultrason. Ferroelectr. Freq. Control,* vol. 52, pp. 578–580, 2005.

[29] M. Kupnik A. Ergun, H. Huang, and B. T. Khuri-Yakub, "6F-2 extended insulation layer structure for CMUTs," in *Proc. of 2007 IEEE International Ultrasonics Symposium* (*IUS*), 2007, pp. 511-514.

[30] M. Kupnik, M. Ho, S. Vaithilingam, and B. T. Khuri-Yakub, "CMUTs for air coupled ultrasound with improved bandwidth," in *Proc. of* 2011 *IEEE International Ultrasonics Symposium* (*IUS*)*,* 2011, pp. 592–595.

[31] J. Hernandez, T. Zure, and S. Chowdhury, "Capacitance measurements of an SOI based CMUT," in *Proc. of IEEE Fourth Latin American Symposium on Circuits and Systems (LASCAS),* 2013, pp. 1-4.

[32] S. Senturia, Microsystems Design; Kluwer Academic Publisher: Norwell, MA, USA, 2000.

[33] S. Upadhyay, "A MEMS Planar Fresnel Lens for CMUT Array," Master's thesis, Electrical and computer Engineering Department, University of Windsor, Windsor, ON, Canada, 2023.

[34] Z. Mehmood, I. Hanif, and F. Udrea, "Material selection for optimum design of MEMS pressure sensors," *Microsystem Technologies*, vol. 26, pp. 2751–2766, Sept. 2020.

[35] N. Andraskar, G. Tiwari, and M. Goel, "Impact response of ceramic structures - A review," *Ceramics International*, vol. 48, pp. 27262–27279, Oct. 2022.

[36] B. Joshi et al., "LPCVD and PECVD silicon nitride for microelectronics technology," *Indian Journal of Engineering and Materials Sciences*, vol. 7, pp. 303-309, Oct. 2000.

[37] M. Madou, Fundamentals of Microfabrication, CRC Press, Boca raton, FL, 1997.

[38] L. Warren, F. Rong, E. Poindexter, G. Gerardi, and J. Kanicki, "Structural identification of the silicon and nitrogen dangling-bond centers in amorphous silicon nitride," *Journal of Applied Physics,* vol. 70, pp. 346–354, Jul. 1991.

[39] D. Krick, P. Lenahan, and J. Kanicki, "Stable photoinduced paramagnetic defects in hydrogenated amorphous silicon nitride," *Applied Physics. Letters*, vol. 51, pp. 608-610, Aug. 1987

[40] P. Lenahan and S. Curry, "First observation of the Si hyperfine spectra of silicon dangling bond centers in silicon nitride," *Applied Physics Letters*, vol. 56, pp. 157, Jan. 1990.

[41] Y. Zhou and P. Zhang, "Theory of field emission from dielectric coated surfaces," *Phys. Rev. Research*, vol. 2, p. 043439, Dec. 2020,

[42] R. Apodaca, "Electrical Characterization of Silicon-Rich Nitride and Silicon Oxynitride Films Deposited by Low-Pressure Chemical Vapor Deposition," Master's Thesis, Department of Electrical Engineering, University of New Mexico, Albuquerque, NM, 2005.